INORGANIC CHEMISTRY
FRONTIERS

RESEARCH ARTICLE

View Article Online
View Journal | View Issue

Cite this: *Inorg. Chem. Front.*, 2024, **11**, 1890

Partial substitution with a significant effect: coexistence of a wide band gap and large birefringence in the oxychalcogenide $AEGe_2O_4Se$ (AE = Sr and Ba)†

Mao-Yin Ran,[a,b,c] Sheng-Hua Zhou,[a,b,c] Wen-Bo Wei,[a,b,c] A-Yang Wang,[a,b,d] Xin-Tao Wu,[a,b] Hua Lin *[a,b] and Qi-Long Zhu *[a,b]

Received 6th December 2023,
Accepted 15th February 2024

DOI: 10.1039/d3qi02509h

rsc.li/frontiers-inorganic

Much effort has been devoted to the discovery of novel birefringent crystals that display considerable birefringence (Δn) in the infrared (IR) region. However, the simultaneous achievement of a wide energy gap (E_g > 3.1 eV) and a large Δn (>0.2) in a heteroanionic chalcogenide system remains a formidable challenge. To address this bottleneck, we applied the partial-substitution strategy and successfully designed and synthesized two new quaternary oxychalcogenides, namely $AEGe_2O_4Se$ (AE = Sr and Ba). These two isomorphic compounds belong to the monoclinic space group $P2_1/c$ (no. 14), featuring a structure composed of two-dimensional (2D) $[Ge_2O_4Se]^{2-}$ layers with an antiparallel arrangement, which are separated by charge-balanced Ba^{2+} cations. Remarkably, they exhibit the coexistence of large Δn values (0.209 and 0.238@2050 nm based on the generalized gradient approximation) and wide E_g values (3.57 and 3.81 eV). Furthermore, theoretical calculations were performed to elucidate the interplay between optical properties and electronic structures. These results reveal that the significantly improved Δn value (approximately 15–17 times that of the parent compound $BaGe_2O_5$) can mainly be attributed to the newly discovered $[GeO_3Se]$ heteroanionic motif. In brief, this study provides a simple chemical substitution method to overcome the trade-off between wide E_g and large Δn values in heteroanionic chalcogenides.

Introduction

Birefringent crystals play an important role in the generation and manipulation of optical polarization, finding widespread applications in laser science and technology. They are particularly significant in optical communications, leading to continuous and comprehensive research efforts.[1] Currently, commercial birefringent materials are primarily composed of oxides, such as YVO_4,[2] $CaCO_3$,[3] and BaB_2O_4.[4] Although these materials exhibit high birefringence (Δn), their application is limited to the ultraviolet and visible range due to the narrow transmission cut-off edge caused by the absorption vibrations of metal–oxygen bonds. Consequently, they cannot be utilized in the infrared (IR) band. Moreover, the pursuit of materials capable of achieving a large Δn plays a critical role in advancing the miniaturization of optical devices.[5] To meet the increasing demands for such materials in laser technology, there is an urgent need to develop new high-performance birefringent crystals, especially for the IR band.

Chalcogenides are classical candidates for photoelectric functional materials in the IR region, with crystal structures predominantly composed of tetrahedral building units.[6] However, the weak polarization anisotropy of these rigid building units often leads to smaller Δn, which limits their comprehensive application.[7] During the past decade, several effective structural design strategies have been employed to address these issues,[8] including: (1) introducing other groups containing lone-pair electrons,[9] (2) introducing π-conjugated units,[10] and (3) exploring new functional building units (FBUs) with significant anisotropy.[11] Although the strategies mentioned above have achieved some crystal materials with high Δn values, an ideal birefringent chalcogenide also needs to consider another key parameter: the transmission range. This parameter is typically dependent on the optical energy gap (E_g) of chalcogenides, which, in turn, determines the range of

[a]*State Key Laboratory of Structural Chemistry, Fujian Institute of Research on the Structure of Matter, Chinese Academy of Sciences, Fuzhou 350002, China. E-mail: linhua@fjirsm.ac.cn, qlzhu@fjirsm.ac.cn*
[b]*Fujian Science & Technology Innovation Laboratory for Optoelectronic Information of China, Fuzhou, Fujian 350108, China*
[c]*University of Chinese Academy of Sciences, Beijing 100049, China*
[d]*College of Chemistry, Fuzhou University, Fujian 350002, China*

†Electronic supplementary information (ESI) available: Additional experimental and theoretical results together with additional tables and figures. CCDC 2301111 and 2301112. For ESI and crystallographic data in CIF or other electronic format see DOI: https://doi.org/10.1039/d3qi02509h

applications for chalcogenides. However, the different requirements for the microstructure of materials due to large Δn and wide E_g values make it difficult for these characteristics to coexist simultaneously in the same material. Therefore, how to effectively achieve a balance between large Δn (>0.2) and wide E_g (>3.1 eV) values is currently a difficult and hot research topic in this system.

Oxychalcogenides containing heteroanionic groups have garnered significant attention as a noteworthy category of candidates for IR birefringent crystals.[12] They offer the synthesis of advantageous properties found in both oxides and chalcogenides. This system demonstrates flexible assembly methods and versatile optical performance. The presence of heteroanionic motifs within the structure not only retains the wide E_g value of the parent oxide but also exhibits a large anisotropic polarization index, contributing to the achievement of a high Δn value.[13] For instance, the anisotropy of the heteroanionic [$GeOS_3$] motif is six times that of the tetrahedral [GeO_4] unit and twice that of the [GeS_4] unit.[14] Furthermore, partially substituting oxygen in oxides with chalcogenide elements proves to be an effective approach for attaining oxychalcogenides with substantial Δn values,[15] for example, $Ba_2SnSSi_2O_7$ (0.105@2050 nm, with the original structure being $Ba_2TiSi_2O_8$),[16] $Sr_3Ge_2O_4Te_3$ (0.152@2090 nm, with the original structure being $Sr_2ZnGe_2O_7$),[17] and $Sr_2CdGe_2OS_6$ (0.193@2050 nm, with the original structure being $Sr_2CdGe_2O_7$).[18]

Recently, we have been focusing on the ternary $AE_xM_yO_{x+2y}$ (AE = alkaline-earth metals; M = group 14 elements) system, which displays a diverse range of constituents and phases. This system showcases structural flexibility, ranging from 0D clusters to 3D frameworks, achieved through simple changes in constituents. As a result, it holds potential for designing new oxychalcogenides. Among the various compounds in this system, $AEGe_2O_5$ has captured our attention. Despite its promising two-dimensional (2D) layered structure, which facilitates the attainment of larger Δn, the reality is quite the opposite (the theoretical Δn is much less than 0.02). This is primarily due to the rigid composition of its functional groups, namely tetrahedral [GeO_4] and octahedral [GeO_6]. Inspired by the aforementioned strategies, we implemented the partial-substitution approach and effectively devised and synthesized two novel quaternary oxychalcogenides, namely $AEGe_2O_4Se$ (AE = Sr and Ba). This study encompasses the solid-phase synthesis, structural progression, and optical characteristics of $AEGe_2O_4Se$ (AE = Sr and Ba). Additionally, theoretical calculations were carried out to attain a more comprehensive understanding of the structure–activity relationship.

Results and discussion

$BaGe_2O_5$ [19] crystallizes in the orthorhombic *cmca* (no. 64) space group. Within its structure, the asymmetric unit comprises one independent Ba atom, two Ge atoms, and four O atoms. The basic structural units of $BaGe_2O_5$ can be visualized as comprising [$Ge1O_6$] octahedra and [$Ge2O_4$] tetrahedra (as shown in Fig. 1a). The [$Ge1O_6$] octahedra connect along the *b*-axis to form an infinite chain (Fig. S1†) through corner-sharing O atoms, and the remaining O atoms of the [$Ge1O_6$] octahedra link two [$Ge2O_4$] tetrahedra along the *b*-axis direction to form a 2D layer (Fig. 1b) through edge-sharing O atoms. Ba^{2+} cations located in the interlayer (Fig. 1c) stabilize this structural configuration to maintain charge balance. Unfortunately, the highly symmetric polyhedral shapes resulting from the rigid coordination model limit polarization anisotropy, resulting in a relatively low Δn of $BaGe_2O_5$. It is important to note that the anisotropic polarizability within a material's structure directly affects its Δn property. Therefore, a flexible coordination environment is more favorable for enhancing Δn.[20] Accordingly, the pursuit of flexible FBUs, rather than rigid ones, is being considered as an effective strategy to increase Δn.

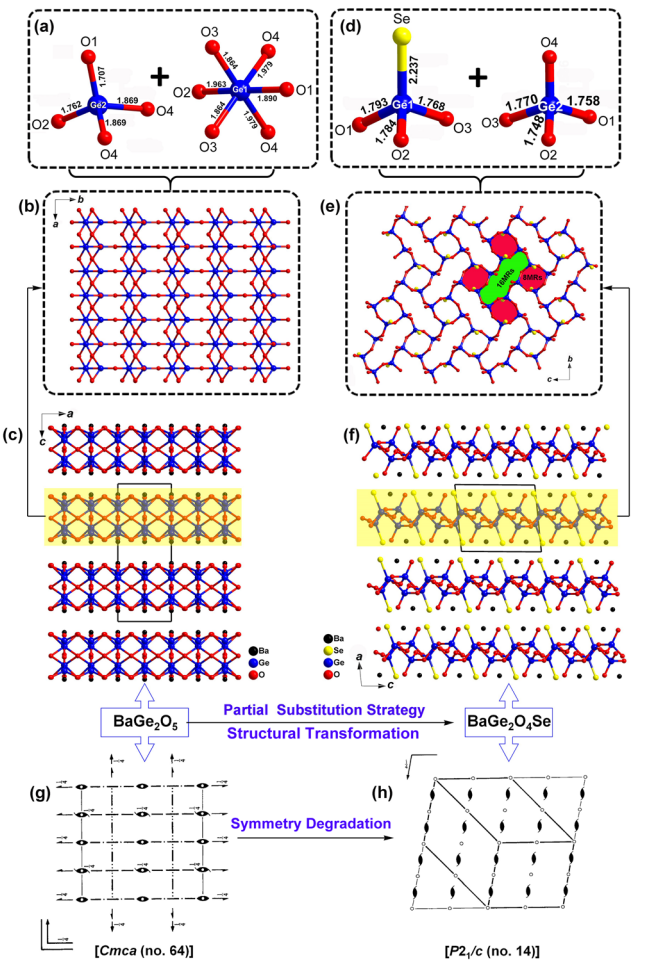

Fig. 1 Structural transformation from oxide $BaGe_2O_5$ to oxychalcogenide $BaGe_2O_4Se$: (a and d) coordination environment of [GeO_4], [GeO_6], and [GeO_3Se] units with the atom numbers outlined; (b and e) 2D $[Ge_2O_5]^{2-}$ and $[Ge_2O_4Se]^{2-}$ anion layers; (c and f) the 2D layered structures viewed from the *b* direction; (g and h) symmetry degradation from *Cmca* (no. 64) to $P2_1/c$ (no. 14).

Oxyselenides, $AEGe_2O_4Se$ (AE = Sr and Ba), represent novel quaternary compounds discovered in AE/M^{IV}/O/Q systems. Due to their isostructural nature, $BaGe_2O_4Se$ is used as a representative compound to describe the crystal structure. $BaGe_2O_4Se$ adopts the monoclinic $P2_1/c$ (no.14) space group, and detailed crystallographic data information can be found in Table 1. The asymmetric unit contains one unique Ba atom, two Ge atoms, four O atoms, and one Se atom, all located at the Wyckoff site 4*e*. The fundamental structure of $BaGe_2O_4Se$ consists of a 2D $[Ge_2O_4Se]^{2-}$ layer, with Ba^{2+} cations filling the interlayer spaces to effectively balance the charge (Fig. 1f). The AE atoms are coordinated with five O atoms and three Se atoms to form $[AEO_5Se_3]$ polyhedra (Fig. S2†). The coordination environment of Ge is depicted in Fig. 1d, and detailed bond lengths and bond angles can be found in Tables S1–S3.† The Ge2 atom is connected to four O atoms, forming $[GeO_4]$ FBUs with Ge–O bond lengths ranging from 1.748 to 1.770 Å. In contrast, the Ge1 atom is linked to three O atoms and one Se atom, forming highly polarized heteroanionic $[GeO_3Se]$ FBUs with Ge–O bond lengths ranging from 1.768 to 1.784 Å and Ge–Se bond lengths of 2.237 Å. The structure further evolves as two $[GeO_3Se]$ FBUs and two $[GeO_4]$ FBUs share edges to create larger building units known as $[Ge_4O_8Se_2]$ 8-membered-rings (8MRs). These 8MRs interconnect, ultimately resulting in the formation of a two-dimensional $[Ge_2O_4Se]^{2-}$ layer through corner-sharing (as illustrated in Fig. 1e). Within this layer, a $[Ge_8O_{16}Se_4]$ 16MR is generated, nestled inside four closely situated $[Ge_4O_8Se_2]$ 8MRs.

The detailed structural evolution from the oxide $BaGe_2O_5$ to the oxychalcogenide $BaGe_2O_4Se$ is depicted in Fig. 1. Both $BaGe_2O_5$ and $BaGe_2O_4Se$ exhibit a similar 2D layered structure. However, there are differences in their FBUs. $BaGe_2O_5$ contains $[GeO_6]$ and $[GeO_4]$ FBUs, and it is evident that these rigidly coordinated FBUs prohibit significant changes in Δn within the parent oxide $BaGe_2O_5$. By introducing Se atoms, which possess different electronegativity and size (χ_O = 3.44 *vs.* χ_{Se} = 2.55), structural modifications are achieved through a partial substitution strategy. In $BaGe_2O_4Se$, the inclusion of flexible coordinated $[GeO_3Se]$ heteroanionic FBUs results in an increased Δn value, which is further supported by experimental observations and theoretical analyses as elaborated below. It is worth noting that in contrast to the previously reported approach of enhancing Δn through a dimensionality reduction strategy, this is the rare instance of improving Δn in an oxychalcogenide system with 2D structures.

Moreover, through a comprehensive comparison and analysis of previously known oxychalcogenides, we have found that $AEGe_2O_4Se$ (AE = Sr and Ba) exhibits the uniqueness of the structure in three categories. Firstly, the distinguishing feature lies in four-coordinated anionic FBUs, denoted as $[GeO_xQ_{4-x}]$.[21–27] This group can be systematically categorized into various subgroups, such as $[GeQ_4]$, $[GeOQ_3]$, $[GeO_2Q_2]$, $[GeO_3Q]$, and $[GeO_4]$, depending on the variation of *x*. In comparative terms, the $[GeOQ_3]$ anionic motif stands out as the most frequently observed, with reports of $[GeOS_3]$,[22] $[GeOSe_3]$,[23] and $[GeOTe_3]$,[24] respectively. The $[GeO_2Q_2]$ FBUs have also been reported, further divided into subgroups like $[GeO_2S_2]$[25] and $[GeO_2Se_2]$.[26] In contrast, $[GeO_3Q]$ FBUs are relatively underrepresented, with the $[GeO_3S]$ FBU only being the primary instances found in some oxychalcogenides.[27] Remarkably, prior to this research, no reports existed regarding the $[GeO_3Se]$ and $[GeO_3Te]$ FBUs. Our study has discovered, for the first time, the heteroanionic $[GeO_3Se]$ FBU, thus enriching the diversity of oxychalcogenides. Additionally, we have also calculated the formation enthalpies of the title compounds,[28] as well as the reported oxyselenides. As shown in Fig. S3,† the formation energies of $SrGe_2O_4Se$ and $BaGe_2O_4Se$ are −1.821 eV per atom and −1.832 eV per atom, respectively, which is even lower compared to most of the reported oxyselenides. This indicates that the title compounds are thermodynamically stable even under zero external pressure. The lack of previous discoveries in this area may be attributed to factors such as the choice of starting material, proportions, and the temperature program utilized in the reaction. Secondly, we have observed that the $[GeO_xQ_{4-x}]$ FBUs tend to exist largely independently within oxythiogermanate compounds. A notable exception to this trend is the compound $Ba_3M^{II}Ge_3O_2S_8$ (M^{II} = Mn, Cd),[29] in which we have recently discovered the coexistence of $[GeOS_3]$ and $[GeO_2S_2]$. This simultaneous presence of different motifs is a relatively rare phenomenon within the context of $[GeO_4]$/$[GeQ_4]$ and $[GeO_xQ_{4-x}]$ FBUs. Additionally, we have uncovered another interesting occurrence where $[GeO_4]$ and $[GeO_3Se]$ FBUs are both present within the same structural framework. Thirdly, our research introduces the most oxygen-rich system within the realm of AE–M^{IV}–O–Q systems reported thus far. This system, namely AE–M^{IV}_2–O_4–Q, offers a novel approach for designing wide energy gap oxychalcogenides.

$AEGe_2O_4Se$ (AE = Sr and Ba) was synthesized through high-temperature solid-phase synthesis, using a stoichiometric ratio of AE (Sr and Ba), Se, and GeO_2 at 1223 K. Millimeter-sized

Table 1 Crystal data and structural refinement details of $AEGe_2O_4Se$ (AE = Sr and Ba)

Empirical formula	$SrGe_2O_4Se$	$BaGe_2O_4Se$
CCDC	2301112	2301111
Formula weight	375.76	425.48
Temperature(K)	293(2)	293(2)
Crystal system	Monoclinic	Monoclinic
Space group	$P2_1/c$ (no. 14)	$P2_1/c$ (no. 14)
a (Å)	6.7668(4)	7.0948(3)
b (Å)	9.5262(5)	9.5602(3)
c (Å)	8.2232(5)	8.4161(3)
β (°)	95.729(5)	95.978(4)
V (Å^3)	527.44(5)	567.74(4)
Z	4	4
D_c (g·cm^{-3})	4.732	4.978
μ (mm^{-1})	28.212	23.708
GOOF on F^2	1.095	1.124
R_1, wR_2 ($I > 2\sigma(I)$)[a]	0.0440, 0.1155	0.0294, 0.0864
R_1, wR_2 (all data)	0.0480, 0.1175	0.0307, 0.0874
Largest diff. peak and hole (e·Å^{-3})	1.23, −2.63	1.115, −2.151

[a] $R_1 = \sum||F_o| - |F_c||/\sum|F_o|$, $wR_2 = [\sum w(F_o^2 - F_c^2)^2/\sum w(F_o^2)^2]^{1/2}$.

single crystals were chosen for testing and characterization purposes. The powder XRD results were in agreement with the results obtained from single crystal test simulations, confirming the purity of the $AEGe_2O_4Se$ (AE = Sr and Ba) phase (Fig. S4†). EDX elemental analysis demonstrated that the AE/Ge/O/Se ratio was well consistent with the results based on the single crystal tests (Fig. S5 and S6†). Moreover, $AEGe_2O_4Se$ (AE = Sr and Ba) exhibited excellent thermal stability under a N_2 atmosphere below 1100 K (Fig. S7†), as there were no observed melting or phase transition features in the corresponding TG-DTA curves. Furthermore, both $SrGe_2O_4Se$ and $BaGe_2O_4Se$ displayed a wide IR transmission cut-off edge at 13.3 and 13.5 μm, respectively (Fig. 2a and b), indicating their potential as birefringent materials for IR applications. It is apparent that there is a prominent absorption peak near 9 μm, which could be attributed to the multi-phonon absorption. A comparable occurrence has also been observed in the infrared transmission spectra of recently reported chalcogenides.[30] The optical E_g value of $AEGe_2O_4Se$ was determined through UV-vis-NIR diffuse reflectance spectra. The calculated E_g values using the Kubelka–Munk function[31] were found to be 3.57 and 3.81 eV for $SrGe_2O_4Se$ and $BaGe_2O_4Se$, respectively (Fig. 2c and d).

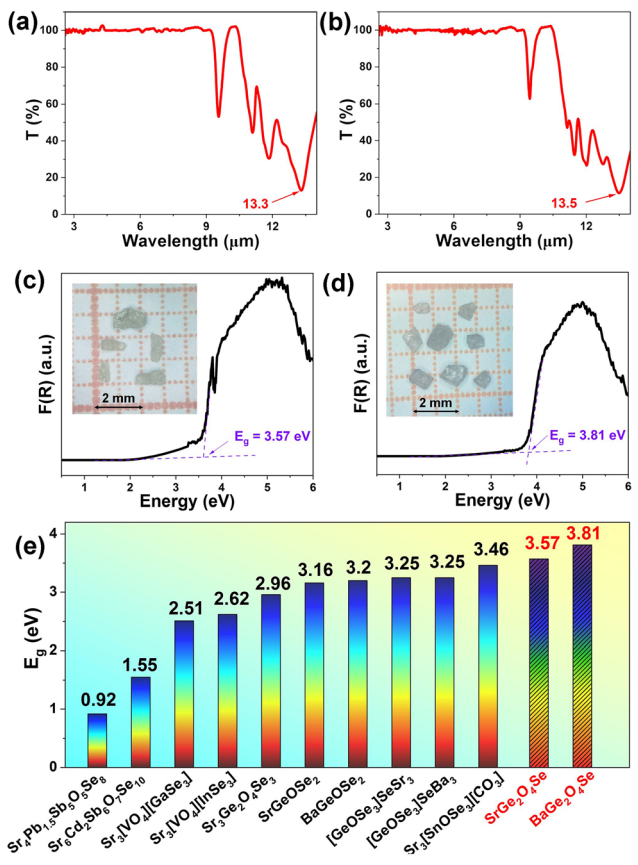

Fig. 2 Optical property characterization of $AEGe_2O_4Se$ (AE = Sr and Ba): (a and b) IR transmittance spectra; (c and d) UV–vis–NIR absorption spectra (inset: photographs of crystals); (e) comparison of the experimental E_g value of reported oxyselenides.

Importantly, these values are the highest among all known oxyselenides (Fig. 2e).[32]

To determine the Δn values of $AEGe_2O_4Se$ (AE = Sr and Ba) in our experiment, we performed Δn measurements on specific crystals based on a ZEISS Axio A1 cross-polarizing microscope equipped with a Berek compensator. For $SrGe_2O_4Se$, we found that the retardation (R-value) was 1.649 μm and the crystal thickness (T-value) was 10.37 μm. Similarly, for $BaGe_2O_4Se$, the corresponding values were determined to be 0.895 μm and 7.67 μm. According to the formula $\Delta n = R/T$,[33] the measured Δn values for $SrGe_2O_4Se$ and $BaGe_2O_4Se$ were 0.16 and 0.12, respectively (Fig. 3). These Δn values are bigger than those of many commercial birefringent crystals, such as MgF_2 (0.012@632 nm),[34] $LiNbO_3$ (0.08@632 nm),[35] and BaB_2O_4 (Δn = 0.122@546 nm).[4] Additionally, they are also larger than those of several typical chalcogenides, including $[Ba_4(S_2)][ZnGa_4S_{10}]$ (0.053@1064 nm),[36] $NaSrBS_3$ (0.137@546 nm),[37] and $K_2Na_2Sn_3S_8$ (0.070@546 nm).[38]

To gain a comprehensive understanding of the electronic structure and optical properties of $AEGe_2O_4Se$ (AE = Sr and Ba), we conducted detailed theoretical studies based on the DFT method. As displayed in Fig. 4a and b, $AEGe_2O_4Se$ (AE = Sr and Ba) exhibits an indirect E_g with calculated values being 1.95 and 2.18 eV, respectively. These values are lower than the experimental results obtained from the solid-state spectra (3.57 and 3.81 eV). This deviation mainly stems from the limited accuracy of traditional DFT functions in E_g calculations.[39] The partial density of states (PDOS) reveals that the valence band maximum (VBM) is predominantly influenced by Se-4p and O-2p orbitals, whereas the conduction band minimum (CBM) is mainly associated with the vacant Ge-3s

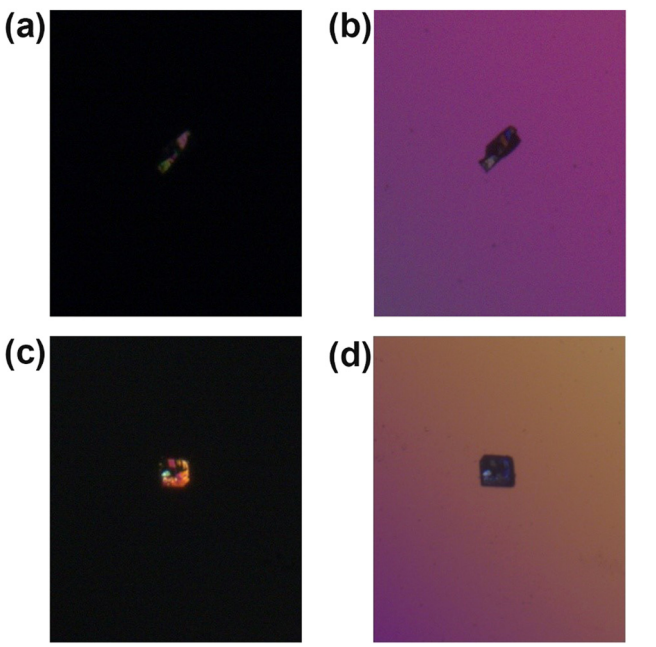

Fig. 3 Changes in the interference color of (a and b) $SrGe_2O_4Se$ and (c and d) $BaGe_2O_4Se$ crystals before and after complete extinction.

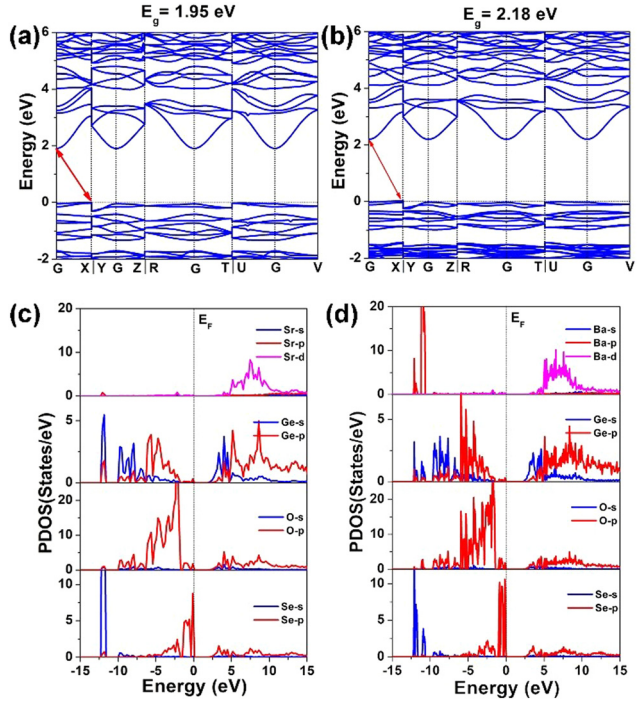

Fig. 4 Theoretical calculated results of $AEGe_2O_4Se$ (AE = Sr and Ba): (a and b) electronic band structures and (c and d) PDOS curves.

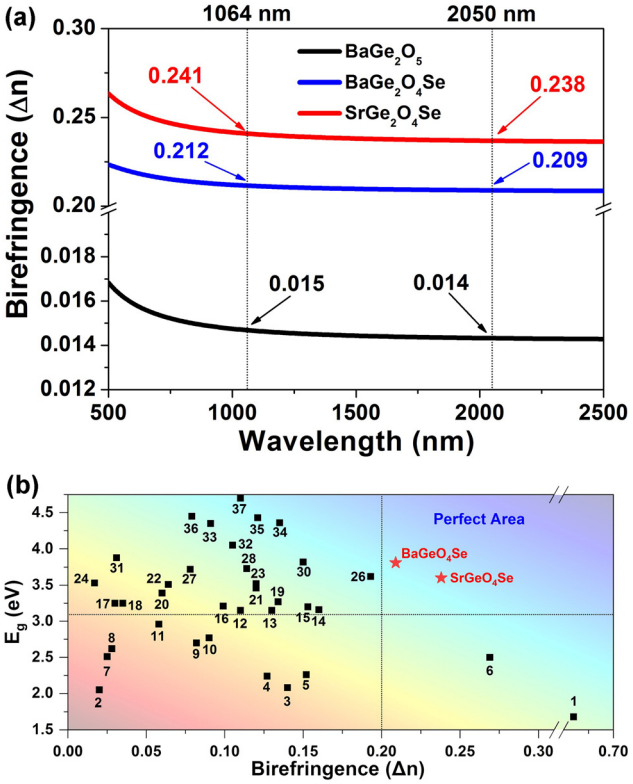

Fig. 5 (a) Calculated birefringence (Δn) of oxide $BaGe_2O_5$ and oxychalcogenide $AEGe_2O_4Se$ (AE = Sr and Ba); (b) comparison of the experimental E_g and calculated Δn values of known oxychalcogenides (1–37) listed in Table S4.†

and Ge-3p orbitals (Fig. 4c and d). The AE atoms make minimal contributions around the E_F and act as balanced charges to stabilize the 2D layered structure. Consequently, the E_g value of $AEGe_2O_4Se$ (AE = Sr and Ba) is primarily influenced by the heteroanionic $[GeO_3Se]$ FBUs, specifically the 2D $[Ge_2O_4Se]^{2-}$ layer.

Additionally, we employed the DFT method to calculate the Δn value of $AEGe_2O_4Se$ (AE = Sr and Ba). The calculated results show Δn values of 0.238 and 0.209@2050 nm, and 0.241 and 0.212@1064 nm for $SrGe_2O_4Se$ and $BaGe_2O_4Se$, respectively (Fig. 5a). The calculated values are larger than the measured Δn values due to the fact that only crystal wafers can be measured in a cross-polarizing microscope, resulting in smaller measured values than the Δn of the material. Furthermore, the parent $BaGe_2O_5$ exhibits a low Δn value of 0.014@2050 nm and 0.015@1064 nm. Notably, partial substitution is an effective strategy in designing birefringent materials with enhanced Δn values.

Based on the above discussion, $AEGe_2O_4Se$ not only undergoes a structural transition from the parent $BaGe_2O_5$ but also exhibits excellent optical properties. These achievements can be attributed to the presence of heteroanionic $[GeO_3Se]$ FBUs at two levels. In comparison with other reported oxychalcogenides (see Table S4† for details), a two-dimensional diagram (Fig. 5b) was plotted, showing the horizontal axis representing the "perfect area" in the graph (Δn) with values greater than 0.2 (representing most commercial materials) and the vertical axis (E_g) exceeds 3.1 eV (corresponding to the cut-off edge of the ultraviolet band at 400 nm). Notably, $AEGe_2O_4Se$ (AE = Sr and Ba) exhibits a coexistence of large calculated Δn values (0.209 and 0.238@2050 nm) and wide experimental E_g values (3.57 and 3.81 eV), indicating their potential as birefringent crystals in the ultraviolet–visible–infrared band.[40]

Conclusions

In summary, we have successfully discovered a new type of quaternary phase in the $AE/M^{IV}/O/Q$ system, namely $AEGe_2O_4Se$ (AE = Sr and Ba), through a partial substitution strategy from the parent $BaGe_2O_5$. These structures feature a unique 2D $[Ge_2O_4Se]^{2-}$ layer formed by the first discovered heteroanionic $[GeO_3Se]$ motif. Comparing the structures of $AEGe_2O_4Se$ (AE = Sr and Ba) a the parent $BaGe_2O_5$, similar layered structures but different FBUs have been observed, indicating a successful structural transformation and optimization achieved through partial Se substitution for O. Furthermore, $AEGe_2O_4Se$ (AE = Sr and Ba) exhibits excellent optical properties, including a wide IR transparent region (13.3–13.5 μm), high Δn values (0.209–0.238@2050 nm) and large E_g values (3.57–3.81 eV). These properties suggest that $AEGe_2O_4Se$ crystals hold promise as candidates for IR birefringent materials. Further investigation into the structure–property relationship reveals that the excellent birefringent properties can be attribu-

ted to the significant structural anisotropy of heteroanionic [GeO_3Se] groups. Overall, this work highlights the oxychalcogenide system as a promising source of IR birefringent crystals, presenting a new route for exploring IR birefringent crystals with well-balanced comprehensive properties.

Author contributions

Mao-Yin Ran: investigation, formal analysis, and writing – original draft. Sheng-Hua Zhou: investigation, methodology, and validation. Wen-Bo Wei: formal analysis and validation. A-Yang Wang: formal analysis and validation. Xin-Tao Wu: conceptualization and writing – review & editing. Hua Lin: supervision, conceptualization, and writing – review & editing. Qi-Long Zhu: supervision and writing – review & editing.

Conflicts of interest

There are no conflicts to declare.

Acknowledgements

This research was supported by the National Natural Science Foundation of China (21771179), the Fujian Science & Technology Innovation Laboratory for Optoelectronic Information of China (2021ZR118), and the Natural Science Foundation of Fujian Province (2022L3092 and 2023H0041).

References

1 (*a*) Z. Xie, L. Sun, G. Han and Z. Gu, Optical Switching of a Birefringent Photonic Crystal, *Adv. Mater.*, 2008, **20**, 3601–3604; (*b*) N. Berti, S. Coen, M. Erkintalo and J. Fatome, Extreme waveform compression with a nonlinear temporal focusing mirror, *Nat. Photonics*, 2022, **16**, 822–827; (*c*) Y. Zhou, X. Zhang, M. Hong, J. Luo and S. Zhao, Achieving effective balance between bandgap and birefringence by confining π-conjugation in an optically anisotropic crystal, *Sci. Bull.*, 2022, **67**, 2276–2279; (*d*) M. Mutailipu, J. Han, Z. Li, F. M. Li, J. J. Li, F. F. Zhang, X. F. Long, Z. H. Yang and S. L. Pan, Achieving the full-wavelength phase-matching for efficient nonlinear optical frequency conversion in $C(NH_2)_3BF_4$, *Nat. Photonics*, 2023, **17**, 694–701; (*e*) F. Zhang, X. Chen, M. Zhang, W. Jin, S. Han, Z. Yang and S. Pan, An excellent deep-ultraviolet birefringent material based on $[BO_2]_\infty$ infinite chains, *Light: Sci. Appl.*, 2022, **11**, 252; (*f*) X. Dong, L. Huang, H. Zeng, Z. Lin, K. M. Ok and G. Zou, High-Performance Sulfate Optical Materials Exhibiting Giant Second Harmonic Generation and Large Birefringence, *Angew. Chem., Int. Ed.*, 2022, **61**, e202116790; (*g*) P.-F. Li, C.-L. Hu, F. Kong and J.-G. Mao, The First UV Nonlinear Optical Selenite Material: Fluorination Control in $CaYF(SeO_3)_2$ and $Y_3F(SeO_3)_4$, *Angew. Chem., Int. Ed.*, 2023, **62**, e202301420.

2 H. Luo, T. Tkaczyk, E. Dereniak and K. Oka, High birefringence of the yttrium vanadate crystal in the middle wavelength infrared, *Opt. Lett.*, 2006, **31**, 616–618.

3 G. Ghosh, Dispersion-equation coefficients for the refractive index and birefringence of calcite and quartz crystals, *Opt. Commun.*, 1999, **163**, 95–102.

4 G. Zhou, J. Xu, X. Chen, H. Zhong and F. Gan, Growth and spectrum of a novel birefringent α-BaB_2O_4 crystal, *J. Cryst. Growth*, 1998, **191**, 517–519.

5 S. Niu, J. Graham, H. Zhao, Y. Zhou, O. Thomas, H. Huaixun, S. Jad, M. Krishnamurthy, U. Brittany and J. Wu, Giant optical anisotropy in a quasi-one-dimensional crystal, *Nat. Photonics*, 2018, **12**, 392–396.

6 H. Chen, M. Y. Ran, W. B. Wei, X. T. Wu, H. Lin and Q. L. Zhu, A comprehensive review on metal chalcogenides with three-dimensional frameworks for infrared nonlinear optical applications, *Coord. Chem. Rev.*, 2022, **470**, 214706.

7 (*a*) M. Zhou, C. Li, X. Li, J. Yao and Y. Wu, $K_2Sn_2ZnSe_6$, $Na_2Ge_2ZnSe_6$, and $Na_2In_2GeSe_6$: A New Series of Quaternary Selenides with Intriguing Structural Diversity and Nonlinear Optical Properties, *Dalton Trans.*, 2016, **45**, 7627–7633; (*b*) M. Y. Li, Y. X. Zhang, H. Lin, Z. J. Ma, X. T. Wu and Q. L. Zhu, Combined experimental and theoretical investigations of Ba_3GaS_4I: interesting structure transformation originated from the halogen substitution, *Dalton Trans.*, 2019, **48**, 17588–17593; (*c*) M. Y. Ran, Z. Ma, X. T. Wu, H. Lin and Q. L. Zhu, $Ba_2Ge_2Te_5$: a ternary NLO-active telluride with unusual one-dimensional helical chains and giant second-harmonic-generation tensors, *Inorg. Chem. Front.*, 2021, **8**, 4838–4845.

8 (*a*) A. Tudi, S. Han, Z. Yang and S. Pan, Potential optical functional crystals with large birefringence: Recent advances and future prospects, *Coord. Chem. Rev.*, 2022, **459**, 214380; (*b*) Q. Shi, L. Dong and Y. Wang, Evaluating refractive index and birefringence of nonlinear optical crystals: Classical methods and new developments, *Chin. J. Struct. Chem.*, 2023, **42**, 100017; (*c*) Y. Long, X. Dong, L. Huang, H. Zeng, Z. Lin, L. Zhou and G. Zou, $BaSb(H_2PO_2)_3Cl_2$: An Excellent UV Nonlinear Optical Hypophosphite Exhibiting Strong Second-Harmonic Generation Response, *Mater. Today Phys.*, 2022, **28**, 100876.

9 (*a*) H. Lin, Y. Y. Li, M. Y. Li, Z. J. Ma, L. M. Wu, X. T. Wu and Q. L. Zhu, Centric-to-acentric structure transformation induced by a stereochemically active lone pair: a new insight for design of IR nonlinear optical materials, *J. Mater. Chem. C*, 2019, **7**, 4638–4643; (*b*) S. Han, A. Tudi, W. Zhang, X. Hou, Z. Yang and S. Pan, Recent Development of Sn(II), Sb(III)-based Birefringent Material: Crystal Chemistry and Investigation of Birefringence, *Angew. Chem., Int. Ed.*, 2023, **62**, e202302025; (*c*) C. Liu, S.-H. Zhou, C. Zhang, Y.-Y. Shen, X.-Y. Liu, H. Lin and Y. Liu, $CsCu_3SbS_4$: rational design of a two-dimensional layered material with giant birefringence derived from Cu_3SbS_4, *Inorg. Chem. Front.*, 2022, **9**, 478–484;

(*d*) C. Zhang, M.-Y. Ran, X. Chen, S.-H. Zhou, H. Lin and Y. Liu, Stereochemically active lone-pair-driven giant enhancement of birefringence from three-dimensional $CsZn_4Ga_5Se_{12}$ to two-dimensional $CsZnAsSe_3$, *Inorg. Chem. Front.*, 2023, **10**, 3367–3374; (*e*) P.-F. Li, J.-G. Mao and F. Kong, A survey of stereoactive oxysalts for linear and nonlinear optical applications, *Mater. Today Phys.*, 2023, **37**, 101197; (*f*) P.-F. Li, C.-L. Hu, J.-G. Mao and F. Kong, A UV Non-Hydrogen Pure Selenite Nonlinear Optical Material Achieving Balanced Properties through Framework-Optimized Structural Transformation, *Mater. Horiz.*, 2024, DOI: 10.1039/D3MH01790G.

10 (*a*) X. Y. Zhang, X. G. Du, J. H. Wang, F. Y. Wang, F. Liang, Z. G. Hu, Z. S. Lin and Y. C. Wu, $K_3C_6N_7O_3{\cdot}2H_2O$: A Multifunctional Nonlinear Optical Cyamelurate Crystal with Colossal π-Conjugated Orbitals, *ACS Appl. Mater. Interfaces*, 2022, **14**, 53074–53080; (*b*) Y. Li, X. Zhang, J. Zheng, Y. Zhou, W. Huang, Y. Song, H. Wang, X. Song, J. Luo and S. Zhao, A Hydrogen Bonded Supramolecular Framework Birefringent Crystal, *Angew. Chem., Int. Ed.*, 2023, **62**, e202304498.

11 (*a*) J. Zhou, L. Wang, Y. Chu, H. Wang, S. Pan and J. Li, Na_3SiS_3F: A Wide Bandgap Fluorothiosilicate with Unique SiS_3F Unit and High Laser-Induced Damage Threshold, *Adv. Opt. Mater.*, 2023, **11**, 2300736; (*b*) M.-Y. Ran, S.-H. Zhou, W.-B. Wei, B.-X. Li, X.-T. Wu, H. Lin and Q.-L. Zhu, Breaking through the Trade-Off between Wide Band Gap and Large SHG Coefficient in Mercury-based Chalcogenides for IR Nonlinear Optical Application, *Small*, 2024, **20**, 2304563; (*c*) A.-Y. Wang, S.-H. Zhou, M.-Y. Ran, X.-T. Wu, H. Lin and Q.-L. Zhu, Regulating the key performance parameters for Hg-based IR NLO chalcogenides via bandgap engineering strategy, *Chin. Chem. Lett.*, 2024, **35**, 109377; (*d*) P.-F. Li, Y.-P. Gong, C.-L. Hu, B. Zhang, J.-G. Mao and F. Kong, Four UV Transparent Linear and Nonlinear Optical Materials Explored from Pure Selenite Compounds, *Adv. Opt. Mater.*, 2023, **11**, 2301426.

12 (*a*) Y. F. Shi, W. Wei, X. T. Wu, H. Lin and Q. L. Zhu, Recent progress in oxychalcogenides as IR nonlinear optical materials, *Dalton Trans.*, 2021, **50**, 4112–4118; (*b*) J. J. Xu and K. Wu, Comprehensive review on multiple mixed-anion ligands, physicochemical performances and application prospects in metal oxysulfides, *Coord. Chem. Rev.*, 2023, **486**, 215139; (*c*) Y. Zhang, H. Wu, Z. Hu and H. Yu, Oxychalcogenides: A Promising Materials Class for Nonlinear Optical Crystals with Mixed-anion Groups, *Chem. – Eur. J.*, 2022, **29**, e202203597; (*d*) J.-X. Zhang, P. Feng, M.-Y. Ran, X.-T. Wu, H. Lin and Q.-L. Zhu, *Coord. Chem. Rev.*, 2024, **502**, 215617.

13 (*a*) J. Guo, A. Tudi, S. Han, Z. Yang and S. Pan, Sn_2PO_4I: an excellent birefringent material with giant optical anisotropy in non π-conjugated phosphate, *Angew. Chem., Int. Ed.*, 2021, **60**, 24901–24904; (*b*) Y. Hu, C. Wu, X. Jiang, Z. Wang, Z. Huang, Z. Lin, X. Long, M. G. Humphrey and C. Zhang, Giant Second-Harmonic Generation Response and Large Band Gap in the Partially Fluorinated Mid-Infrared Oxide $RbTeMo_2O_8F$, *J. Am. Chem. Soc.*, 2021, **143**, 12455–12459; (*c*) Y. Deng, L. Huang, X. Dong, L. Wang, K. M. Ok, H. Zeng, Z. Lin and G. Zou, $K_2Sb(P_2O_7)F$: Cairo pentagonal layer with bifunctional genes reveal optical performance, *Angew. Chem., Int. Ed.*, 2020, **59**, 21151–21156.

14 R. Wang, F. Liang, X. Liu, Y. Xiao, Q. Liu, X. Zhang, L. M. Wu, L. Chen and F. Huang, Heteroanionic Melilite Oxysulfide: A Promising Infrared Nonlinear Optical Candidate with a Strong Second-Harmonic Generation Response, Sufficient Birefringence, and Wide Bandgap, *ACS Appl. Mater. Interfaces*, 2022, **14**, 23645–23652.

15 (*a*) H. Lin, W. B. Wei, H. Chen, X. T. Wu and Q. L. Zhu, Rational design of infrared nonlinear optical chalcogenides by chemical substitution, *Coord. Chem. Rev.*, 2020, **406**, 213150; (*b*) M. Y. Ran, A. Y. Wang, W. B. Wei, X. T. Wu, H. Lin and Q. L. Zhu, Recent progress in the design of IR nonlinear optical materials by partial chemical substitution: structural evolution and performance optimization, *Coord. Chem. Rev.*, 2023, **481**, 215059; (*c*) H. D. Yang, M. Y. Ran, W. B. Wei, X. T. Wu, H. Lin and Q. L. Zhu, Recent advances in IR nonlinear optical chalcogenides with well-balanced comprehensive performance, *Mater. Today Phys.*, 2023, **35**, 101127.

16 Y. Shi, Z. Ma, B. Li, X. Wu, H. Lin and Q. Zhu, Phase matching achieved by isomorphous substitution in IR nonlinear optical material $Ba_2SnSSi_2O_7$ with an undiscovered $[SnO_4S]$ functional motif, *Mater. Chem. Front.*, 2022, **6**, 3054–3061.

17 M. Sun, W. Xing, M. Lee and J. Yao, Bridging oxygen atoms in trigonal prism units driven strong second-harmonic-generation efficiency in $Sr_3Ge_2O_4Te_3$, *Chem. Commun.*, 2022, **58**, 11167–11170.

18 M. Y. Ran, S. H. Zhou, B. Li, W. Wei, X. T. Wu, H. Lin and Q. L. Zhu, Enhanced Second-Harmonic-Generation Efficiency and Birefringence in Melilite Oxychalcogenides $Sr_2MGe_2OS_6$ (M = Mn, Zn, and Cd), *Chem. Mater.*, 2022, **34**, 3853–3861.

19 M. Ozima, J. Susaki, S. Akimoto and Y. Shimizu, The system $BaOGeO_2$ at high pressures and temperatures, with special reference to high-pressure transformations in $BaGeO_3$, $BaGe_2O_5$, and $Ba_2Ge_5O_{12}$, *J. Solid State Chem.*, 1982, **44**, 307–317.

20 (*a*) J. Xu, Y. Xiao, K. Wu, B. Zhang, D. Lu, H. Yu and H. Zhang, Flexible Anionic Groups-Activated Structure Dissymmetry for Strong Nonlinearity in $Ln_2Ae_3M^{IV}{}_3S_{12}$ Family, *Small*, 2024, **20**, 2306577; (*b*) Y. Huang, Y. Zhang, D. Chu, Z. Yang, G. Li and S. Pan, HgB_2S_4: A d^{10} Metal Thioborate with Giant Birefringence and Wide Band Gap, *Chem. Mater.*, 2023, **35**, 4556–4563; (*c*) G. Li, Z. Yang, X. Hou and S. Pan, Chain-like $[S_x]$ (x = 2–6) Units Realizing Giant Birefringence with Transparency in the Near-Infrared for Optoelectronic Materials, *Angew. Chem., Int. Ed.*, 2023, **62**, e202303711.

21 J. Xu, K. Wu, Y. Xiao, B. Zhang, H. Yu and H. Zhang, Mixed-AnionOriented Design of $LnMGa_3S_6O$ (Ln = La, Pr, and Nd; M = Ca and Sr) Nonlinear Optical Oxysulfides with

Targeted Property Balance, *ACS Appl. Mater. Interfaces*, 2022, **14**, 37967–37974.

22 (*a*) N. Zhang, Q. Xu, Z. Shi, M. Yang and S. Guo, Characterizations and Nonlinear-Optical Properties of Pentanary Transition-Metal Oxysulfide $Sr_2CoGe_2OS_6$, *Inorg. Chem.*, 2022, **61**, 17002–17006; (*b*) H. D. Yang, S. H. Zhou, M. Y. Ran, X. T. Wu, H. Lin and Q. L. Zhu, Melilite oxychalcogenide $Sr_2FeGe_2OS_6$: a phase-matching IR nonlinear optical material realized by isomorphous substitution, *Inorg. Chem. Front.*, 2023, **10**, 2030.

23 W. Xing, P. Fang, N. Wang, Z. Li, Z. Lin, J. Yao, W. Yin and B. Kang, Two Mixed-Anion Units of $[GeOSe_3]$ and $[GeO_3S]$ Originating from Partial Isovalent Anion Substitution and Inducing Moderate Second Harmonic Generation Response and Large Birefringence, *Inorg. Chem.*, 2020, **59**, 16716–16724.

24 M. Sun, W. Xing, M. Lee and J. Yao, Bridging oxygen atoms in trigonal prism units driven strong second-harmonic-generation efficiency in $Sr_3Ge_2O_4Te_3$, *Chem. Commun.*, 2022, **58**, 11167–11170.

25 (*a*) X. Zhang, Y. Xiao, R. Wang, P. Fu, C. Zheng and F. Huang, Synthesis, crystal structures and optical properties of noncentrosymmetric oxysulfides $AeGeS_2O$ (Ae = Sr, Ba), *Dalton Trans.*, 2019, **48**, 14662–14668; (*b*) H. Yang, S. Zhou, M. Ran, X. Wu, H. Lin and Q. Zhu, Oxychalcogenides as Promising Ultraviolet Nonlinear Optical Candidates: Experimental and Theoretical Studies of $AEGeOS_2$ (AE = Sr and Ba), *Inorg. Chem.*, 2022, **61**, 15711–15720.

26 (*a*) M. Y. Ran, Z. J. Ma, H. Chen, B. X. Li, X. T. Wu, H. Lin and Q. L. Zhu, Partial Isovalent Anion Substitution to Access Remarkable Second-Harmonic Generation Response: A Generic and Effective Strategy for Design of Infrared Nonlinear Optical Materials, *Chem. Mater.*, 2020, **32**, 5890–5896; (*b*) B. Liu, X. Jiang, G. Wang, H. Zeng, M. Zhang, S. Li, W. Guo and G. Guo, Oxychalcogenide $BaGeOSe_2$: Highly Distorted Mixed-Anion Building Units Leading to a Large Second-Harmonic Generation Response, *Chem. Mater.*, 2015, **27**, 8189–8192.

27 H. Liu, Z. Song, H. Wu, Z. Hu, J. Wang, Y. Wu and H. Yu, $[Ba_2F_2][Ge_2O_3S_2]$: An Unprecedented Heteroanionic Infrared Nonlinear Optical Material Containing Three Typical Anions, *ACS Mater. Lett.*, 2022, **4**, 1593–1598.

28 C. A. Niedermeier, J.-I. Yamaura, J. Wu, X. He, T. Katase, H. Hosono and T. Kamiya, Crystal Structure Built from a GeO_6–GeO_5 Polyhedra Network with High Thermal Stability: β–$SrGe_2O_5$, *ACS Appl. Electron. Mater.*, 2019, **1**, 1989–1993.

29 S. H. Zhou, M. Y. Ran, W. Wei, A. Y. Wang, X. T. Wu, H. Lin and Q. L. Zhu, Heteroanion-introduction-driven birefringence enhancement in oxychalcogenide $Ba_3M^{II}Ge_3O_2S_8$ (M^{II} = Mn, Cd), *Inorg. Chem. Front.*, 2023, **10**, 5997–6004.

30 (*a*) Z. Li, S. Zhang, Z. Huang, L.-D. Zhao, E. Uykur, W. Xing, Z. Lin, J. Yao and Y. Wu, Molecular Construction from $AgGaS_2$ to $CuZnPS_4$: Defect-Induced Second Harmonic Generation Enhancement and Cosubstitution-Driven Band Gap Enlargement, *Chem. Mater.*, 2020, **32**, 3288–3296; (*b*) M.-Y. Li, Z. Ma, B. Li, X.-T. Wu, H. Lin and Q.-L. Zhu, $HgCuPS_4$: An Exceptional Infrared Nonlinear Optical Material with Defect Diamond-like Structure, *Chem. Mater.*, 2020, **32**, 4331–4339; (*c*) Y. Chu, P. Wang, H. Zeng, S. Cheng, X. Su, Z. Yang, J. Li and S. Pan, $Hg_3P_2S_8$: A New Promising Infrared Nonlinear Optical Material with a Large Second-Harmonic Generation and a High Laser-Induced Damage Threshold, *Chem. Mater.*, 2021, **33**, 6514–6521.

31 (*a*) P. Kubelka, Ein beitrag zur optik der farbanstriche, *J. Tech. Phys.*, 1931, **12**, 593; (*b*) M. A. Butler, Photoelectrolysis and physical properties of the semiconducting electrode WO_2, *J. Appl. Phys.*, 1977, **48**, 1914.

32 (*a*) Y. Wang, M. Luo, P. Zhao, X. Che, Y. Cao and F. Huang, $Sr_4Pb_{1.5}Sb_5O_5Se_8$: a new mid-infrared nonlinear optical material with a moderate SHG response, *CrystEngComm*, 2020, **22**, 3526–3530; (*b*) R. Wang, F. Wang, X. Zhang, X. Feng, C. Zhao, K. Bu, Z. Zhang, T. Zhai and F. Q. Huang, Improved Polarization in the $Sr_6Cd_2Sb_6O_7Se_{10}$ Oxyselenide through Design of Lateral Sublattices for Efficient Photoelectric Conversion, *Angew. Chem., Int. Ed.*, 2022, **61**, e202206816; (*c*) R. Wang, F. Liang, X. Zhang, Y. Yang and F. Huang, Synthesis, structural evolution and optical properties of a new family of oxychalcogenides $[Sr_3VO_4][MQ_3]$(M = Ga, In, Q = S, Se), *Inorg. Chem. Front.*, 2022, **9**, 4768–4775; (*d*) J. K. Wang, Y. S. Cheng, H. P. Wu, Z. G. Hu, J. Y. Wang, Y. C. Wu and H. W. Yu, $Sr_3[SnOSe_3][CO_3]$: A Heteroanionic Nonlinear Optical Material Containing Planar p-conjugated $[CO_3]$ and Heteroleptic $[SnOSe_3]$ Anionic Groups, *Angew. Chem., Int. Ed.*, 2022, **61**, e202201616.

33 Y. X. Chen, Z. X. Chen, Y. Zhou, Y. Q. Li, Y. C. Liu, Q. R. Ding, X. Chen, S. G. Zhao and J. H. Luo, An Antimony (III) Fluoride Oxalate With Large Birefringence, *Chem. – Eur. J.*, 2021, **27**, 4557–4560.

34 M. J. Dodge, Refractive properties of magnesium fluoride, *Appl. Opt.*, 1984, **23**, 1980–1985.

35 D. E. Zelmon, D. L. Small and D. Jundt, Infrared corrected Sellmeier coefficients for congruently grown lithium niobate and 5 mol% magnesium oxide-doped lithium niobate, *J. Opt. Soc. Am. B*, 1997, **14**, 3319–3322.

36 K. Ding, H. Wu, Z. Hu, J. Wang, Y. Wu and H. Yu, $[Ba_4(S_2)][ZnGa_4S_{10}]$: Design of an Unprecedented Infrared Nonlinear Salt-Inclusion Chalcogenide with Disulfide-Bonds, *Small*, 2023, **19**, 2302819.

37 Y. Yun, M. Wu, C. Xie, Z. Yang, G. Li and S. Pan, Theoretical Prediction-Assisted Synthesis and Characterization of Infrared Nonlinear Optical Material $NaSrBS_3$, *Adv. Opt. Mater.*, 2023, **11**, 2300256.

38 X. Ji, H. Wu, B. Zhang, H. Yu, Z. Hu, J. Wang and Y. Wu, Intriguing Dimensional Transition Inducing Variable Birefringence in $K_2Na_2Sn_3S_8$ and $Rb_3NaSn_3Se_8$, *Inorg. Chem.*, 2021, **60**, 1055–1061.

39 P. E. Blochl, Projector augmented-wave method, *Phys. Rev. B: Condens. Matter*, 1994, **50**, 17953–17979.

40 (*a*) R. Wang, F. Liang, F. Wang, Y. Guo, X. Zhang, Y. Xiao, K. Bu, Z. Lin, J. Yao, T. Zhai and F. Huang, $Sr_6Cd_2Sb_6O_7S_{10}$:

Strong SHG Response Activated by Highly Polarizable Sb/O/S Groups, *Angew. Chem., Int. Ed.*, 2019, **58**, 8078–8081; (*b*) M. Y. Ran, S. H. Zhou, W. Wei, B. Li, X. T. Wu, H. Lin and Q. L. Zhu, Rational Design of a Rare-Earth Oxychalcogenide $Nd_3[Ga_3O_3S_3][Ge_2O_7]$ with Superior Infrared Nonlinear Optical Performance, *Small*, 2023, **19**, 2300248; (*c*) J. N. Li, X. H. Li, Y. X. Xu, W. L. Liu and S. P. Guo, First Investigation of Nonlinear Optical Oxychalcogenide with Three-Dimensional Anionic Framework and Special Windmill-Like Functional Motifs, *Chin. J. Chem.*, 2022, **40**, 2407–2414; (*d*) Y. Cheng, H. Wu, H. Yu, Z. Hu, J. Wang and Y. Wu, Rational Design of a Promising Oxychalcogenide Infrared Nonlinear Optical Crystal, *Chem. Sci.*, 2022, **13**, 5305–5310; (*e*) Y. Shi, S. Zhou, P. Liu, X. Wu, H. Lin and Q. Zhu, Unique $[Sb_6O_2S_{13}]^{12-}$ finite chain in oxychalcogenide $Ba_6Sb_6O_2S_{13}$ leading to ultra-low thermal conductivity and giant birefringence, *Inorg. Chem. Front.*, 2023, **10**, 4425–4434.